

# OH-initiated oxidation of benzene

## Part II.† Influence of elevated NO<sub>x</sub> concentrations

Björn Klotz,\*‡<sup>a</sup> Rainer Volkamer,<sup>b</sup> Michael D. Hurley,<sup>c</sup> Mads P. Sulbaek Andersen,<sup>d</sup>  
Ole John Nielsen,<sup>e</sup> Ian Barnes,<sup>f</sup> Takashi Imamura,<sup>a</sup> Klaus Wirtz,<sup>g</sup> Karl-Heinz Becker,<sup>f</sup>  
Ulrich Platt,<sup>b</sup> Timothy J. Wallington<sup>c</sup> and Nobuaki Washida<sup>h</sup>

<sup>a</sup> National Institute for Environmental Studies, Atmospheric Environment Division, 16-2 Onogawa, Tsukuba-shi, Ibaraki-ken 305-8506, Japan. E-mail: bjoern.klotz@nies.go.jp

<sup>b</sup> Universität Heidelberg, Institut für Umweltphysik, Im Neuenheimer Feld 229, D-69120, Heidelberg, Germany

<sup>c</sup> Ford Motor Co., 20000 Rotunda Drive, Mail Drop SRL-3083, Dearborn, Michigan 48121-2053, USA

<sup>d</sup> University of Southern Denmark, Department of Chemistry, Campusvej 55, DK-5230, Odense M, Denmark

<sup>e</sup> Department of Chemistry, University of Copenhagen, Universitetsparken 5, DK-2100, Copenhagen, Denmark

<sup>f</sup> Bergische Universität Wuppertal, Physikalische Chemie - FB 9, Gaußstraße 20, D-42097, Wuppertal, Germany

<sup>g</sup> Fundación Centro de Estudios Ambientales del Mediterraneo (CEAM), Parque Tecnológico, Calle Charles R. Darwin 14, E-46980, Paterna (Valencia), Spain

<sup>h</sup> Kyoto University, Department of Chemistry, Graduate School of Science, Sakyo-ku, Kyoto 606-8502, Japan

Received 7th May 2002, Accepted 10th July 2002

First published as an Advance Article on the web 13th August 2002

The present work represents a continuation of part I of this series of papers, in which we investigated the phenol yields in the OH-initiated oxidation of benzene under conditions of low to moderate concentrations of NO<sub>x</sub>, to elevated NO<sub>x</sub> levels. The products of the OH-initiated oxidation of benzene in 700–760 Torr of N<sub>2</sub>/O<sub>2</sub> diluent at 297 ± 4 K were investigated in 3 different photochemical reaction chambers. *In situ* spectroscopic techniques were employed for the detection of products, and the initial concentrations of benzene, NO<sub>x</sub>, and O<sub>2</sub> were widely varied (by factors of 6300, 1500, and 13, respectively). In contrast to results from previous studies, a pronounced dependence of the product distribution on the NO<sub>x</sub> concentration was observed. The phenol yield decreases from approximately 50–60% in the presence of low concentrations (<5 ppb) of NO<sub>x</sub> to values below 5% in the presence of extremely high (>10 000 ppb) NO<sub>x</sub> concentrations. In the presence of high concentrations of NO<sub>x</sub>, the phenol yield increases with increasing O<sub>2</sub> partial pressure. The rate constant of the reaction of hydroxycyclohexadienyl peroxy radicals with NO was determined to be  $(1.7 \pm 0.6) \times 10^{-11} \text{ cm}^3 \text{ molecule}^{-1} \text{ s}^{-1}$ . This reaction leads to the formation of *E,E*-2,4-hexadienedial as the main identifiable product (29 ± 16%). The reaction of the hydroxycyclohexadienyl radical with NO<sub>2</sub> gave phenol (5.9 ± 3.4%) and *E,E*-2,4-hexadienedial (3.4 ± 1.9%), no other products could be identified. The residual FTIR product spectra indicate the formation of unknown nitrates or other nitrogen-containing species in high yield. The results from the present work also show that experimental studies aimed at establishing/verifying chemical mechanisms for aromatic hydrocarbons must be performed using NO<sub>x</sub> levels which are representative of those found in the atmosphere.

### 1. Introduction

The importance of aromatic hydrocarbons in local and regional air pollution is well established.<sup>1</sup> Aromatic hydrocarbons contribute significantly to the formation of ozone and secondary organic aerosols in urban air.<sup>1,2</sup> An understanding of the atmospheric chemistry of aromatic compounds is therefore crucial for our understanding of the chemistry governing air

pollution. Unfortunately, despite numerous studies, substantial uncertainties persist in our understanding of the atmospheric chemistry of aromatic compounds, making them a priority field for mechanistic studies.<sup>3,4</sup> The simplest aromatic hydrocarbon, benzene, reacts exclusively with OH radicals under tropospheric conditions. This reaction is rather slow when compared to those of alkylbenzenes, the rate constant  $k_{\text{OH}+\text{benzene}} = 1.2 \times 10^{-12} \text{ cm}^3 \text{ molecule}^{-1} \text{ s}^{-1}$  is a factor of five to fifty lower than  $k_{\text{OH}}$  of toluene and trimethylbenzenes, respectively.<sup>5</sup> The relatively low reactivity of benzene gives rise to a significant residence time in the atmosphere (several weeks) and consequently a rather low photochemical activity. Benzene oxidation is therefore not a major source of

† For Part I see ref. 7.

‡ Present address: Bergische Universität Wuppertal, Physikalische Chemie - FB9, Gaußstraße 20, D-42097, Wuppertal, Germany. E-mail: E-mail: bjoern.klotz@uni-wuppertal.de

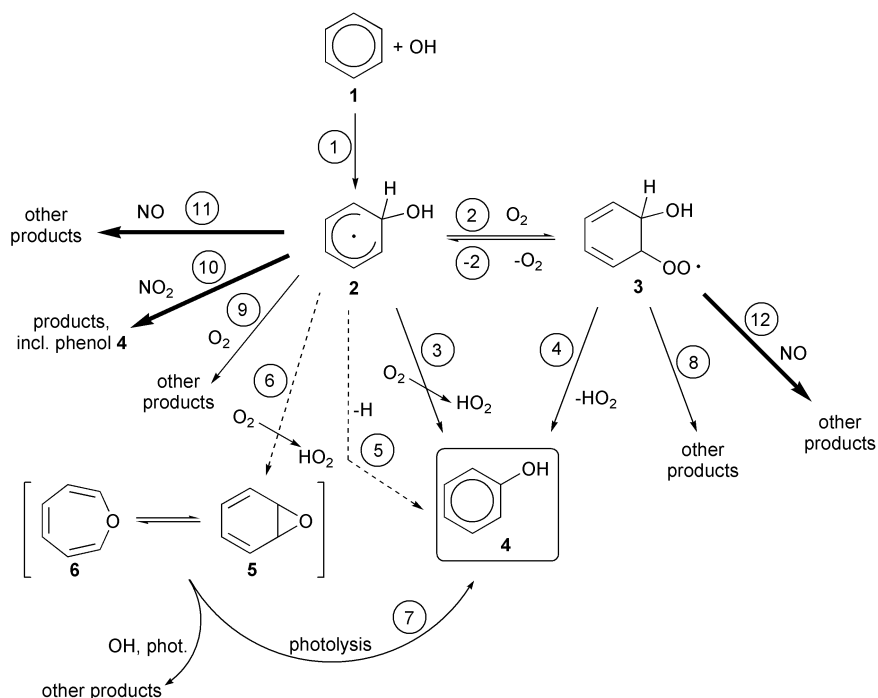


**Fig. 1** Proposed pathways for the initial steps in the OH-radical initiated degradation of benzene in the gas-phase. Thick lines indicate the pathways studied in this work, thin lines those studied by Volkamer *et al.*<sup>7</sup> and dashed lines those probably not operative.<sup>7</sup> "Other products" denotes products other than phenol.

photooxidants in urban air. However, there is another incentive to study the benzene + OH reaction. At ambient temperatures this reaction proceeds almost exclusively *via* addition of OH to the aromatic ring, see reaction (1) of Fig. 1. The general mechanistic conclusions from benzene studies serve as a model for the OH addition pathway for the alkylated monocyclic aromatics, which are considerably more reactive.<sup>6</sup>

In part I of this series, Volkamer *et al.*<sup>7</sup> extensively reviewed the initial steps of benzene oxidation and investigated the formation of phenol under atmospheric conditions (*i.e.* low to moderate NO<sub>x</sub> levels). In Fig. 1 these initial steps are re-drawn to summarize our previous conclusions and illustrate the connection of the present work to part I. Briefly, addition of OH results in the formation of a hydroxycyclohexadienyl radical **2**, which under atmospheric conditions will reversibly add O<sub>2</sub> to give a hydroxycyclohexadienyl peroxy radical **3**. This equilibrium adjusts rapidly<sup>8</sup> and a multitude of subsequent reaction channels have been proposed, see reactions (3)–(12) in Fig. 1. Under most atmospheric conditions species **2** and **3** are lost predominately *via* reactions involving molecular oxygen through channels (3), (4), (6), (8) and (9).<sup>8,9</sup> Of these, channels (3) and (4) lead to the formation of phenol. Volkamer *et al.*<sup>7</sup> presented a method to distinguish both pathways on the basis of temperature dependent considerations and concluded that the majority of phenol is probably formed *via* channel (3). The experimental evidence<sup>10</sup> for channel (5) has been disputed<sup>8,11,12</sup> and it is unlikely that this pathway is actually operative. Channel (6) is now believed to be of minor, or negligible, importance.<sup>7,13,14</sup>

In the presence of high concentrations of NO<sub>x</sub> channels (10), (11) and (12) become significant loss processes for species **2/3**. Channel (11) is negligible under all but the most extreme laboratory conditions.<sup>9,15</sup> Channels (10) and (12) are important loss processes for species **2/3** at NO<sub>x</sub> concentrations above 0.1 ppm<sup>8,9</sup> (parts per million, 1 ppm = 2.46 × 10<sup>13</sup> cm<sup>-3</sup> at standard temperature and pressure). The dependence of the phenol formation yield on the NO<sub>x</sub> concentration has the potential to offer valuable insights into the various further

degradation channels of **2/3**. The formation of phenol following OH initiated oxidation of benzene in the presence of several ppm NO<sub>x</sub> was investigated by Atkinson *et al.*,<sup>16</sup> but no significant dependence of the phenol yield on NO<sub>x</sub> concentration was found and a phenol yield of (23.6 ± 4.4)% was reported. In recent studies by Bjergbakke *et al.*<sup>10</sup> and Berndt *et al.*,<sup>13</sup> phenol yields of (25 ± 5)% and (23 ± 7)%, respectively, were reported. These later studies were conducted under NO<sub>x</sub> free conditions, apparently confirming the absence of a NO<sub>x</sub> dependence of the phenol yield. Similar results were obtained by Berndt and Böge,<sup>17</sup> who reported results of an investigation of the OH initiated degradation of benzene as a function of NO<sub>x</sub> concentration, pressure and temperature.

However, our re-calibration<sup>7</sup> of the studies of Bjergbakke *et al.*<sup>10</sup> and Berndt *et al.*<sup>13</sup> showed that considerable scatter exists among the apparently conclusive values if the data are placed on a common basis of calibration.<sup>18</sup> Further, we determined the phenol yield from the reaction of benzene with OH radicals under realistic atmospheric conditions to be (53.1 ± 6.6)%.<sup>7</sup> Part of that difference of more than a factor of two was attributed to the influence of channels (10) and (12) which were expected to decrease the phenol yield under conditions of elevated NO<sub>x</sub>. However, for high NO<sub>x</sub> conditions (several ppm) the predicted dependence of the phenol yield on the NO<sub>x</sub> concentration was found to contrast with the rather constant yield found by Atkinson *et al.*<sup>16</sup>

Here we investigate the formation of phenol and hexadienals in the OH-initiated oxidation of benzene under conditions where the loss processes of **2/3** are dominated by reactions involving NO<sub>x</sub> rather than oxygen. Even though such conditions are unlikely to be observed in the atmosphere, they have been widely applied in smog chamber studies in the past. The objective of this study is to elucidate whether the reaction steps drawn in Fig. 1 allow a general description of the initial steps of benzene oxidation in the presence of NO<sub>x</sub>. The NO, NO<sub>2</sub> and oxygen concentrations were varied systematically to differentiate between these reaction channels and to obtain insight into their products.

## 2. Experimental

The experimental data reported herein were obtained using three different experimental facilities; indoor photoreactors at NIES in Tsukuba/Japan and at FORD in Dearborn/USA, and an outdoor chamber (EUPHORE) at CEAM in Valencia/Spain. Detailed descriptions of the EUPHORE,<sup>7,19</sup> NIES<sup>7,20</sup> and FORD<sup>21</sup> facilities are available in the literature.

### 2.1 NIES reaction chamber

The NIES photochemical reaction chamber is a 6.065 m<sup>3</sup> Teflon-coated steel vessel with a surface/volume ( $S/V$ ) ratio of 3.7 m<sup>-1</sup>. It is equipped with a high-performance pump system for efficient cleaning and can be temperature controlled over the range 15–90 °C. The light source is a solar simulator that consists of nineteen 1 kW high pressure Xe arc lamps which were operated at 80% of their maximum power. The lamps are fitted with 2 mm Pyrex glass filters (cutoff wavelength 290 nm) to simulate the sunlight reaching the lower troposphere. The photolysis frequency of NO<sub>2</sub> in this system is  $J(\text{NO}_2) = 4.25 \times 10^{-3} \text{ s}^{-1}$ , while that of methyl nitrite is  $J(\text{CH}_3\text{ONO}) = 8.7 \times 10^{-4} \text{ s}^{-1}$ .

Concentrations of reactants and products were determined using an FTIR spectrometer Nicolet Nexus 670, which was operated at a spectral resolution of 1 cm<sup>-1</sup> and coupled to a White-type mirror system allowing an absorption path of 221.5 m. The spectrometer was equipped with a liquid nitrogen cooled MCT (mercury cadmium tellurium) detector.

### 2.2 EUPHORE reaction chamber

The outdoor European Photo-Reactor (EUPHORE) is part of the Centro de Estudios Ambientales del Mediterraneo (CEAM), located near Valencia/Spain. The hemispherical FEP chamber used in the present study had a volume of *ca.* 187 m<sup>3</sup> and an  $S/V$  ratio of 1 m<sup>-1</sup>. FTIR spectrometry and differential optical absorption spectroscopy (DOAS) were the primary analytical techniques employed. The irradiation source for the experiments is natural sunlight.

### 2.3 FORD reaction chamber

The reaction chamber at FORD Motor Co. is an evacuable 140 L Pyrex glass vessel with a surface to volume ratio of 14.4 m<sup>-1</sup>. 22 Fluorescent blacklamps (GE F15T8-BL) provide the light source, the irradiation intensity corresponds to an NO<sub>2</sub> photolysis frequency of  $J(\text{NO}_2) = 1.2 \times 10^{-3} \text{ s}^{-1}$ . Products and reference compounds were monitored *in situ* by FTIR spectroscopy using a spectral resolution of 0.25 cm<sup>-1</sup> and an analysing path-length of 27 m. The experiments were conducted using an O<sub>2</sub> partial pressure of 50–650 Torr in 700 Torr total pressure of N<sub>2</sub> diluent. Experiments were performed at a temperature of (296 ± 2) K.

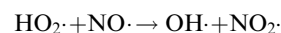
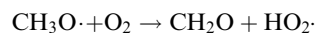
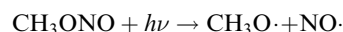
The FTIR and DOAS absorption cross sections used in the evaluations of benzene and phenol in all three laboratories were taken from Etzkorn *et al.*<sup>18</sup> NO and NO<sub>2</sub> were determined by chemiluminescence in the EUPHORE experiments and by FTIR spectrometry at NIES and FORD. Integrated FTIR absorption cross sections of NO and NO<sub>2</sub> were determined independently in both laboratories and were in agreement within 4%.

### 2.4 Types of experiments performed

The experimental type refers to the OH-radical source applied in the different experiments, the nomenclature used is consistent with that used in part I of this series.<sup>7</sup> Initial conditions of the complete data set are listed in Table 1. The experiments performed under low-NO<sub>x</sub> conditions at EUPHORE and

NIES have been discussed previously<sup>7</sup> and are re-stated in Table 1 for ease of reference.

Under the high NO<sub>x</sub> concentrations employed in many of the NIES experiments, the reaction of OH radicals with NO<sub>2</sub> acted as an efficient scavenger of OH, which resulted in very low benzene degradation rates. To alleviate this, most of the high-NO<sub>x</sub> experiments were conducted with added CH<sub>3</sub>ONO (1–2 ppm) (experiment type (6)). In the presence of ultraviolet light, NO and molecular oxygen, methyl nitrite forms OH radicals through the following sequence of reactions:



The NIES benzene/CH<sub>3</sub>ONO/NO<sub>x</sub> experiments can be divided into 2 subgroups. In the first group the NO<sub>x</sub> was largely present as NO initially, and NO to NO<sub>2</sub> conversion occurred during the irradiation. Initial NO concentrations of up to  $2.25 \times 10^{14} \text{ molecule cm}^{-3}$  were employed. These experiments were designed to study the impact of elevated concentrations of NO on the OH-initiated oxidation of benzene. Under these experimental conditions, reaction of the hydroxycyclohexadienyl peroxy radicals **3** with NO was the major loss process for **2/3**. In the second group of experiments a large excess of NO<sub>2</sub> was added to the initial mixture and excess NO<sub>2</sub> was maintained throughout the run. These conditions were designed to investigate the impact of high NO<sub>2</sub> concentrations on the OH-initiated oxidation of benzene, reaction of the hydroxycyclohexadienyl radical **2** with NO<sub>2</sub> would be the dominating loss process of **2/3** here. To scavenge O<sub>3</sub> and NO<sub>3</sub> radicals, NO (*ca.*  $2.5 \times 10^{13} \text{ molecule cm}^{-3}$ ) was added to the high-NO<sub>2</sub> experiments.

In this type of experiment, the photolysis of NO<sub>2</sub> can lead to the formation of significant amounts of ozone, which in turn can react with the excess NO<sub>2</sub> to form NO<sub>3</sub> radicals. Phenol reacts rapidly with NO<sub>3</sub> radicals<sup>22</sup> so the experimental conditions had to be adjusted to minimize the importance of this reaction. Using a simple steady state analysis<sup>19</sup> and the relevant reaction rate coefficients of Atkinson<sup>5</sup> it can be calculated that for experiment NB40, which had the highest average ozone and consequently the highest expected NO<sub>3</sub> concentration, about  $3 \times 10^6 \text{ molecule cm}^{-3}$  of NO<sub>3</sub> are formed. At this concentration the loss of phenol through NO<sub>3</sub> reaction is <5% of that through OH reaction, as calculated from the average OH concentration and the rate constant for the reaction of phenol with OH.<sup>5</sup> Reaction of phenol with NO<sub>3</sub> radicals is therefore concluded to be negligible under the present experimental conditions. Other reactions that might influence the results are those of intermediates with ozone or HO<sub>2</sub>/RO<sub>2</sub> radicals. However, the high NO concentrations employed here effectively suppress the formation of these species in the experiments. In the high-NO<sub>2</sub> experiments, the maximum ozone concentration is around  $10^{12} \text{ molecule cm}^{-3}$ , in the high-NO experiments ozone is not detectable (< $10^{11} \text{ molecule cm}^{-3}$ ). In the low-NO<sub>x</sub> experiments already presented in part I,<sup>7</sup> maximum ozone concentrations reached  $(5\text{--}10) \times 10^{12} \text{ molecule cm}^{-3}$ . Even these comparably high concentrations did not influence the measured phenol yields. Due to the slow build-up and the widely varying maximum concentrations of ozone, product yields would otherwise have been expected to vary considerably, not only between experiments but also within individual runs.

The NIES experiments were performed in (760 ± 20) Torr of purified air at (298 ± 3) K, irradiation times were 2–4 h for the benzene/NO<sub>x</sub> experiments and 45–60 min for the benzene/CH<sub>3</sub>ONO/NO<sub>x</sub> experiments. Spectra were recorded by co-adding 100 scans in the benzene/CH<sub>3</sub>ONO/NO<sub>x</sub> experiments and 270 scans in the benzene/NO<sub>x</sub> experiments. All but 2 of

**Table 1** Summary of the conditions and results of the experiments conducted

Experiment code	Experiment type	[benzene] <sub>initial</sub> / 10 <sup>13</sup> cm <sup>-3</sup>	Tracer compound	[CH <sub>3</sub> ONO] <sub>initial</sub> / 10 <sup>13</sup> cm <sup>-3</sup>	[NO] <sub>avg.</sub> /ppb	[NO <sub>2</sub> ] <sub>avg.</sub> /ppb	Y <sub>phenol</sub> /%	Y <sub>phenol</sub> <sup>corr</sup> /%
<i>NIES</i>								
NBE1	(1)	12.2	Di-n-butyl ether	—	858	170	33.5	33.0 ± 5.4
NBE2	(1a)	12.3	Di-n-butyl ether	0.10	638	350	34.6	33.7 ± 2.9
NBE3	(6)	5.0	—	2.5	1288	627	25.0	23.8 ± 4.9
NBE4	(6)	12.3	Di-n-butyl ether	2.3	1217	835	25.8	24.4 ± 2.1
NB17	(6)	17.8	Di-n-butyl ether	5.3	1606	1634	18.1	15.9 ± 1.4
NB18	(6)	18.4	Di-n-butyl ether	5.2	3686	1687	16.7	15.0 ± 1.4
NB19	(1)	18.6	Di-n-butyl ether	0.02	97	95	42.7	42.4 ± 4.3
NB20	(1)	18.3	Di-n-butyl ether	0.02	35	57	44.8	44.6 ± 5.1
NB21	(1)	18.6	Di-n-butyl ether	0.02	170	123	43.1	42.8 ± 6.4
NB22	(6)	18.5	Di-n-butyl ether	5.2	2734	1509	14.6	12.8 ± 1.3
NB23	(6)	18.4	Di-n-butyl ether	5.2	4294	1789	11.7	10.0 ± 1.3
NB24	(6)	18.8	Di-n-butyl ether	5.5	8426	2032	5.1	3.8 ± 1.8
NB25	(6)	18.2	Di-n-butyl ether	5.3	7681	1844	8.2	6.9 ± 1.8
NB29	(6)	18.1	Di-n-butyl ether	2.7	3678	6172	8.1	4.7 ± 3.7
NB30	(6)	24.6	Di-n-butyl ether	7.2	1320	3660	17.7	14.4 ± 1.7
NB31	(6)	48.2	Di-n-butyl ether	7.5	243	2279	20.5	17.4 ± 1.7
NB32	(6)	48.6	Di-n-butyl ether	7.5	1215	3503	21.5	18.3 ± 1.7
NB33	(6)	48.9	Di-n-butyl ether	7.7	382	1855	20.6	17.8 ± 1.7
NB34	(6)	48.8	Di-n-butyl ether	7.6	446	2451	21.5	18.5 ± 1.5
NB40	(6)	48.6	Di-n-butyl ether	7.6	889	3351	18.6	15.2 ± 1.5
NB41	(6)	42.1	Di-n-butyl ether	7.8	1534	4202	16.6	13.2 ± 1.6
NB42	(6)	48.2	Di-n-butyl ether	7.7	2249	4805	14.9	11.5 ± 1.5
NB43	(1)	24.8	—	0.02	20	41	42.1	42.0 ± 6.9
<i>EUPHORE</i>								
BEN1	(1)	5.8	—	—	18	33	48.0	47.9 ± 6.9
BEN2	(1)	2.9	—	—	54	32	49.9	49.8 ± 10.1
BEN3	(1)	2.9	—	—	84	47	44.4	44.3 ± 11.5
BEN4	(1)	2.9	—	—	60	33	48.8	48.7 ± 7.4
BEN5	(1)	5.7	Di-n-butyl ether	—	100	78	47.7	47.4 ± 5.2
BEN6	(1)	2.8	Di-n-butyl ether	—	135	75	52.1	51.9 ± 4.4
BEN7	(1)	2.8	—	—	124	55	47.4	47.3 ± 6.0
BEN8	(1)	2.9	Di-n-butyl ether	—	25	21	49.6	49.5 ± 4.1
BEN9	(1)	1.2	Di-n-butyl ether	—	65	30	55.3	55.2 ± 5.7
BE10	(1)	2.9	—	—	15	16	55.7	55.6 ± 7.9
BE11	(1)	0.16	—	—	22	19	56.1	56.0 ± 10.6
BE12	(2)	1.0	—	—	2	2	55.8	55.8 ± 7.5
BE13	(2)	0.16	—	—	2	2	58.4	58.4 ± 8.5
BE14	(4)	0.50	—	—	2	2	66.6	66.6 ± 8.1
BE15	(5)	2.4	—	—	1	5	55.0	55.0 ± 7.2
BE16	(1)	8.4	Di-n-butyl ether	—	108	66	48.3	48.1 ± 4.8
BE17	(1)	11.3	Di-n-butyl ether	—	145	86	43.9	43.6 ± 4.4
BE16-II	(5)	2.5	—	—	1	4	56.7	56.6 ± 9.2
BE17-II	(3)	1.4	—	—	64	34	54.5	54.4 ± 4.5
BE18	(3)	2.7	—	—	75	67	50.5	50.3 ± 9.0
BE19	(3)	0.11	—	—	55	30	57.8	57.7 ± 8.5
BE24	(3)	10.6	Mesitylene	—	95	96	50.4	50.1 ± 7.9
BE26	(3)	4.9	Mesitylene	—	62	69	50.3	50.1 ± 5.8
BE28	(3)	44.2	<i>p</i> -Cresol	—	600	191	42.1	41.6 ± 5.2
BE28-II	(3)	41.2	<i>p</i> -Cresol	—	1360	445	26.6	25.7 ± 4.4
BE31 <sup>a</sup>	(3)	37.8	<i>p</i> -Cresol	—	115	110	53.5	53.1 ± 7.0
<i>FORD</i>								
05-14-01 <sup>b</sup>	(6)	961	Propene	327	671	796	20.5	17.5 ± 4.4
05-24-27 <sup>b</sup>	(6)	965	Propene	327	1340	1533	14.1	10.5 ± 1.7
04-30-01	(6)	1000	Propene	330	592	791	31.0	29.3 ± 0.2
02-05-01	(6)	291	Propene	327	1313	1421	22.8	20.6 ± 2.2
04-25-14	(6)	285	Propene	301	1055	1548	21.5	19.1 ± 1.4
05-01-01	(6)	1003	Propene	327	1528	1116	20.5	18.6 ± 1.8
05-11-01 <sup>c</sup>	(6)	971	Propene	314	737	663	35.0	34.6 ± 3.3
01-30-24 <sup>c</sup>	(6)	288	Propene	350	1196	1327	35.8	35.2 ± 3.3

Experiment types: (1) benzene/NO<sub>x</sub>, (1a) benzene/NO<sub>x</sub> with small amount of added CH<sub>3</sub>ONO, (2) ozone-photolysis, (3) HONO photolysis, (4) H<sub>2</sub>O<sub>2</sub> photolysis, (5) HCHO/NO<sub>x</sub> system, (6) benzene/CH<sub>3</sub>ONO/NO<sub>x</sub>.<sup>a</sup> 300 Torr O<sub>2</sub> in 760 Torr, <sup>b</sup> 50 Torr O<sub>2</sub> in 700 Torr, <sup>c</sup> 650 Torr O<sub>2</sub> in 700 Torr, all other experiments are conducted with the atmospheric O<sub>2</sub> mixing ratio of 20% in 700 Torr (FORD) or 760 Torr (NIES, EUPHORE).

the NIES experiments were conducted with an added OH tracer substance (di-n-butyl ether) to determine the concentration–time profile of OH radicals.

All the experiments conducted at FORD were of the benzene/CH<sub>3</sub>ONO/NO<sub>x</sub> type. The OH-radical tracer compound used was propene. Consumption of propene was measured and used to calculate the consumption of benzene. In all experiments benzene consumption was limited to <5%. Mixtures of benzene, propene, CH<sub>3</sub>ONO and NO were subjected to consecutive 1–10 s irradiations. After each irradiation the concentrations of propene, phenol, NO and NO<sub>2</sub> were determined using FTIR spectroscopy. The experimental conditions were chosen so that reactions of propene with O<sub>3</sub> and phenol with NO<sub>3</sub> did not influence the results. The initial concentrations were; benzene, (3–15) × 10<sup>15</sup>; propene, 1.9 × 10<sup>14</sup>; CH<sub>3</sub>ONO, (1–5) × 10<sup>14</sup>, and NO, either 3.2 × 10<sup>13</sup> or 6.5 × 10<sup>13</sup> molecule cm<sup>-3</sup>. Experiments were conducted at 700 Torr total pressure and 3 oxygen concentrations; 50, 140 and 650 Torr (7, 20 and 93%).

The experimental data were evaluated by the methods described previously,<sup>7</sup> the new NIES and the FORD data were evaluated using method (b<sub>2</sub>) therein.

## 2.5 NO<sub>x</sub> dependence of the phenol yield

On the basis of the mechanistic scheme shown in Fig. 1 Volkamer *et al.*<sup>7</sup> derived the following formula to describe the dependence of the phenol yield on the concentrations of NO<sub>x</sub>. The simplifications made in this approach<sup>7</sup> also apply under the high NO<sub>x</sub> conditions discussed in this work and make formula (1) a valid starting point for further discussion:

$$Y_{\text{phenol}} = \frac{\frac{k_3}{K_{\text{eq}}} + k_4 + Y_{\text{phenol}}^{(10)} \frac{k_{10} [\text{NO}_2]}{K_{\text{eq}} [\text{O}_2]}}{\frac{k_3}{K_{\text{eq}}} + \frac{k_9}{K_{\text{eq}}} + k_4 + k_8 + \frac{k_{10} [\text{NO}_2]}{K_{\text{eq}} [\text{O}_2]} + k_{12} [\text{NO}]} \quad (1)$$

In this equation the numerator represents the rate of formation of phenol from reactions (3) and (4) involving oxygen (henceforth  $k_{\text{phenol}} = k_3/K_{\text{eq}} + k_4$ ) and reaction (10) involving NO<sub>2</sub>,  $Y_{\text{phenol}}^{(10)}$  denotes the phenol yield from reaction (10),  $K_{\text{eq}}$  is the equilibrium constant  $K_{\text{eq}} = k_2/k_{-2}$  of the equilibrium reactions (2) and (–2). The denominator represents the total loss rate for the intermediates **2/3** and will be called  $k_{\text{total}}$  for simplification ( $k_{\text{total}}^{-1}$  is equal to the lifetime of **2/3**):

$$Y_{\text{phenol}} = \frac{k_{\text{phenol}} + Y_{\text{phenol}}^{(10)} \frac{k_{10} [\text{NO}_2]}{K_{\text{eq}} [\text{O}_2]}}{k_{\text{total}}} \quad (2)$$

Rearrangement gives:

$$Y_{\text{phenol}} - Y_{\text{phenol}}^{(10)} \frac{k_{10} [\text{NO}_2]}{k_{\text{total}} K_{\text{eq}} [\text{O}_2]} = \frac{k_{\text{phenol}}}{k_{\text{total}}} \quad (3)$$

Under conditions of low concentrations of NO<sub>x</sub>, as prevalent in the atmosphere,  $k_{\text{total}}$  is equal to  $k_{\text{clean}} = (k_3 + k_9)/K_{\text{eq}} + k_4 + k_8 = (760 \pm 80) \text{ s}^{-1}$ .<sup>8</sup>

In evaluations of the experiments, the NO<sub>x</sub> concentrations were taken as the averages over the measurement time. According to eqn. (3) a plot of the phenol yield, corrected for phenol formed in reaction (10), as a function of  $k_{\text{total}}^{-1}$  should yield a straight line through the origin, with a slope equal to the formation rate of phenol from **2/3**,  $k_{\text{phenol}}$ . The ratio of  $k_{\text{phenol}}$  to the total loss rate of **2** and **3** under atmospheric conditions,  $k_{\text{clean}}$ , gives the phenol yield under atmospheric conditions.

## 2.6 Determination of $k_{12}$

The experiments conducted under excess NO concentrations allow the measured phenol formation yields to be used to

determine the rate coefficient for the reaction of the hydroxycyclohexadienyl peroxy radical **3** with NO (reaction (12) in Fig. 1). Under these conditions, reaction (12) will be the dominant loss channel of **2** and **3**. If phenol formation from reaction (10) is negligible, then

$$k_{\text{total}} = k_{\text{phenol}}/Y_{\text{phenol}} \quad (4)$$

The assumption that phenol formation from the reaction of **2** with NO<sub>2</sub> (reaction (10)) does not contribute significantly to the overall phenol formation in these experiments is justified based on (a) the low phenol formation yield in this reaction determined in the present study and (b) the use of only those experiments where NO was added in excess. Reaction (10) will, however, be a non-negligible loss process of **2/3**, and  $k_{\text{total}}$  can be corrected according to:

$$k_{\text{total}}^{\text{NO}_2\text{-corrected}} = k_{\text{total}} - \frac{k_{10} [\text{NO}_2]}{K_{\text{eq}} [\text{O}_2]} = \frac{k_{\text{phenol}}}{Y_{\text{phenol}}} - \frac{k_{10} [\text{NO}_2]}{K_{\text{eq}} [\text{O}_2]} \quad (5)$$

Since, considering the definitions of  $k_{\text{total}}$  and  $k_{\text{clean}}$ ,  $k_{\text{total}}^{\text{NO}_2\text{-corrected}} = k_{\text{clean}} + k_{12} [\text{NO}]$  it follows:

$$\frac{k_{\text{phenol}}}{Y_{\text{phenol}}} - \frac{k_{10} [\text{NO}_2]}{K_{\text{eq}} [\text{O}_2]} = k_{\text{clean}} + k_{12} [\text{NO}] \quad (6)$$

Thus, a plot of  $k_{\text{phenol}}/Y_{\text{phenol}} - k_{10}[\text{NO}_2]/(K_{\text{eq}}[\text{O}_2])$  as a function of the NO concentration should yield a straight line with a slope of  $k_{12}$  and an intercept of  $k_{\text{clean}}$ . The parameters  $k_{10}$ ,  $K_{\text{eq}}$  and  $k_{\text{clean}}$  are available in the literature,<sup>8,9</sup>  $k_{\text{phenol}}$  has been determined in part I of this series<sup>7</sup> and the other parameters are measured directly.

## 2.7 Determination of the phenol yield from reaction (10)

The phenol yield from the reaction of the hydroxycyclohexadienyl radical **2** with NO<sub>2</sub> ( $Y_{\text{phenol}}^{(10)}$ ) can be determined by rearranging eqn. (2):

$$Y_{\text{phenol}}^{(10)} = (Y_{\text{phenol}} k_{\text{total}} - k_{\text{phenol}}) \frac{K_{\text{eq}} [\text{O}_2]}{k_{10} [\text{NO}_2]} \quad (7)$$

Only those experiments conducted in the presence of a large excess of NO<sub>2</sub> were used in the determination of  $Y_{\text{phenol}}^{(10)}$ . In addition, due to the decay of NO<sub>2</sub> during the experiments, only phenol formation yields measured during the initial 15–30 min of the experiments were used. The measured phenol yield between any 2 data points is given by:

$$Y_{\text{phenol}} = \frac{\Delta[\text{phenol}]_{t(n)-t(n-1)}^{\text{corrected}}}{\Delta[\text{benzene}]_{t(n)-t(n-1)}} \quad (8)$$

Here,  $\Delta[\text{phenol}]_{t(n)-t(n-1)}^{\text{corrected}}$  is the amount of phenol formed between times  $t(n-1)$  and  $t(n)$ , corrected for losses through OH-radical reaction and wall deposition, and  $\Delta[\text{benzene}]_{t(n)-t(n-1)}$  is the benzene reacted in the same time interval. The correction of the phenol concentrations was performed as described earlier, see Volkamer *et al.*<sup>7</sup> Combining eqn. (7) and (8) with the definition of  $k_{\text{total}}$  gives the following formula for the phenol yield from reaction (10):

$$Y_{\text{phenol}}^{(10)} (t(n) - t(n-1)) = \left\{ \frac{\Delta[\text{phenol}]_{t(n)-t(n-1)}^{\text{corrected}}}{\Delta[\text{benzene}]_{t(n)-t(n-1)}} \times \left( k_{\text{clean}} + k_{12} [\text{NO}] + \frac{k_{10} [\text{NO}_2]}{K_{\text{eq}} [\text{O}_2]} \right) - k_{\text{phenol}} \right\} \frac{K_{\text{eq}} [\text{O}_2]}{k_{10} [\text{NO}_2]} \quad (9)$$

The time intervals  $t(n-1)$  to  $t(n)$  correspond to the spectra recorded during the experiments. Phenol yields from reaction (10) are calculated for the respective intervals of an experiment and then averaged to calculate  $Y_{\text{phenol}}^{(10)}$  for that experiment. The

average of the yields of the individual experiments is then calculated to give the overall value for  $Y_{\text{phenol}}^{(10)}$ .

For 298 K and tropospheric concentrations of  $\text{O}_2$ , the following kinetic parameters have been reported in the literature:<sup>8,9</sup>  $K_{\text{eq}} = (2.7 \pm 0.4) \times 10^{-19} \text{ cm}^3 \text{ molecule}^{-1}$ ,  $k_{\text{clean}} = (k_3 + k_9)/K_{\text{eq}} + k_4 + k_8 = (760 \pm 80) \text{ s}^{-1}$ ,  $k_{10} = (2.75 \pm 0.2) \times 10^{-11} \text{ cm}^3 \text{ molecule}^{-1} \text{ s}^{-1}$ , and  $k_{12} = (1.1 \pm 0.4) \times 10^{-11} \text{ cm}^3 \text{ molecule}^{-1} \text{ s}^{-1}$ . For  $k_{12}$ , the value determined in the present study has been employed instead of the literature value, see below.

## 2.8 The yields of *E,E*-2,4-hexadienedial from reactions (10) and (12)

*E,E*-2,4-hexadienedial (species **9** in Fig. 2) is a highly reactive unsaturated dicarbonyl, and its steady state concentrations are consequently very low. It reacts rapidly with OH radicals and photolyses under irradiation with ambient sunlight.<sup>23,24</sup> In the OH initiated oxidation of benzene, *E,E*-2,4-hexadienedial can be formed *via* the formation pathways proposed by Zellner *et al.*<sup>25</sup> and Hoshino *et al.*<sup>26</sup> The degradation scheme of *E,E*-2,4-hexadienedial is given in Klotz *et al.*<sup>24</sup> Fig. 2 gives an overview of the postulated formation pathways of 2,4-hexadienedial **9** in reactions (10) and (12), as well as the subsequent degradation mechanism. The degradation scheme involves a reversible photoisomerisation, and photolysis and OH radical reaction of both *E,E*-2,4-hexadienedial and its photoisomerisation product.

Due to the complex behaviour of *E,E*-2,4-hexadienedial **9** it is not possible to derive a simple kinetic equation to calculate its formation yield in the benzene photooxidation system. Therefore the formation yield of *E,E*-2,4-hexadienedial has been fitted to its observed concentration–time profiles using the chemical simulation software FACSIMILE. In the simulation runs, the OH radical concentration–time profiles were fitted to the decay of the added OH tracer substance, concentrations of NO and  $\text{NO}_2$  were fitted to the experimentally

determined values. The chemical scheme was that shown in Fig. 1 and 2, the kinetic parameters for the reactions in Fig. 1 were those given above, the kinetic parameters for the reactions shown in Fig. 2 were taken from Klotz *et al.*<sup>24</sup> Reactions (5), (6), and (11) in Fig. 1 were ignored, see above and Volkamer *et al.*<sup>7</sup>

Since reactions (10) and (12) can both lead to the formation of *E,E*-2,4-hexadienedial, an iterative procedure had to be employed. First approximations for the yield of *E,E*-2,4-hexadienedial **9** from reaction (12) were obtained using the high- $\text{NO}$  experiments (NB17, NB18, NB22–25) and assuming the *E,E*-2,4-hexadienedial yield from reaction (10) to be negligible. The results for the individual experiments were averaged, and that average was used in simulation runs of 3 high- $\text{NO}_2$  experiments (NB40–42) in which the yield of *E,E*-2,4-hexadienedial from reaction (10) was fitted to its observed concentration–time profile. Those yields were then averaged and used to determine a second approximation to the yield of **9** from reaction (12). The iterations were repeated until self-consistency was achieved.

## 3. Results and discussion

An overview of the experiments conducted, their conditions and results is given in Table 1. The experiment type nomenclature is the same as that used in part I.<sup>7</sup> Fig. 3 shows typical FTIR product spectra of the 3 types of experiments performed at NIES, and selected reference spectra. The product spectra are normalised by the benzene consumption, which leads to different levels of spectral noise. Notably a low benzene consumption in (b) causes a relatively high noise level in the normalised spectrum.

In the low- $\text{NO}_x$  experiment (a) the product spectrum is dominated by the absorptions of phenol, a result that is in line with the experiments shown in part I of this series, see Volkamer *et al.*<sup>7</sup> In contrast, as seen in panel (b), very little

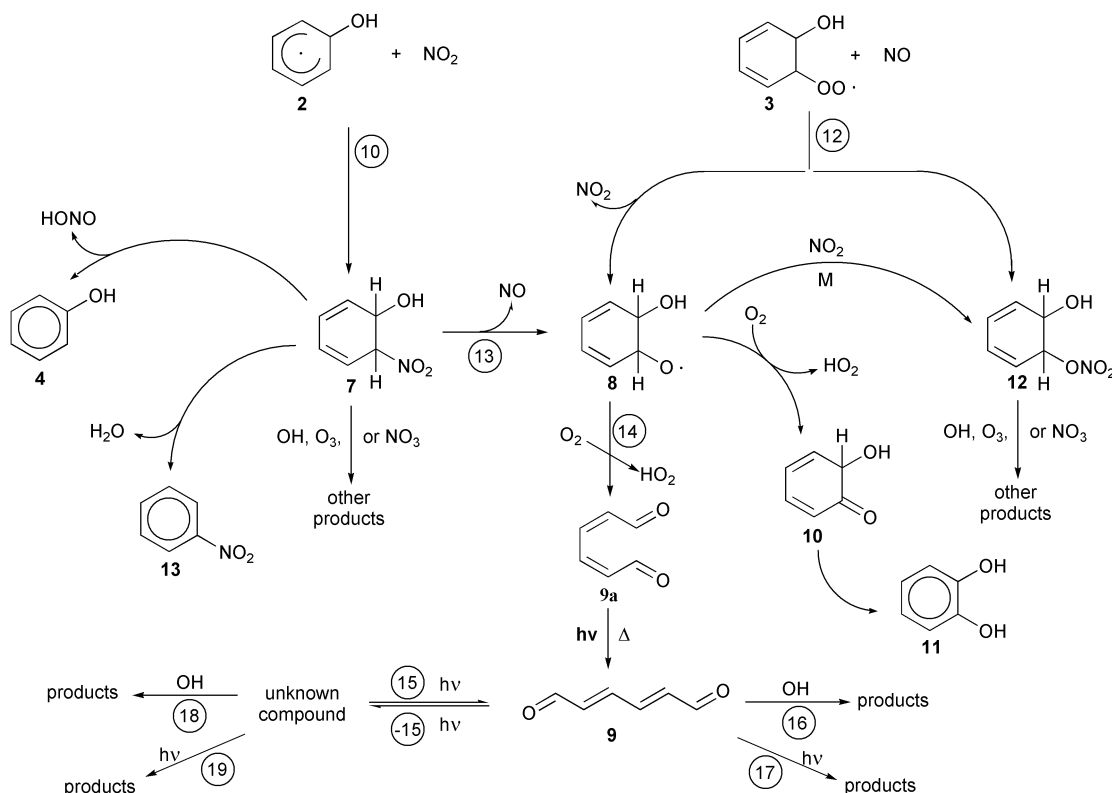
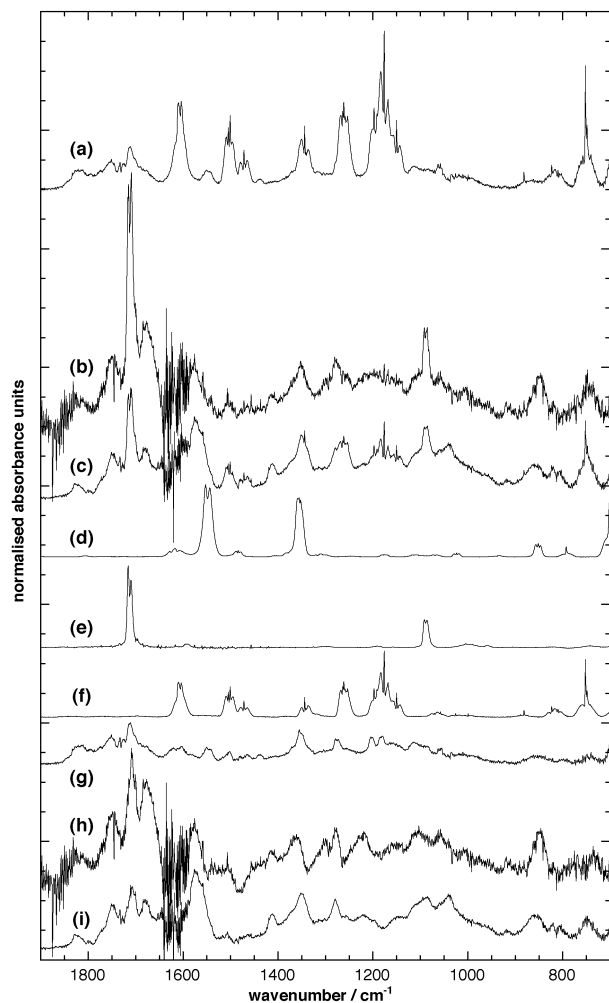
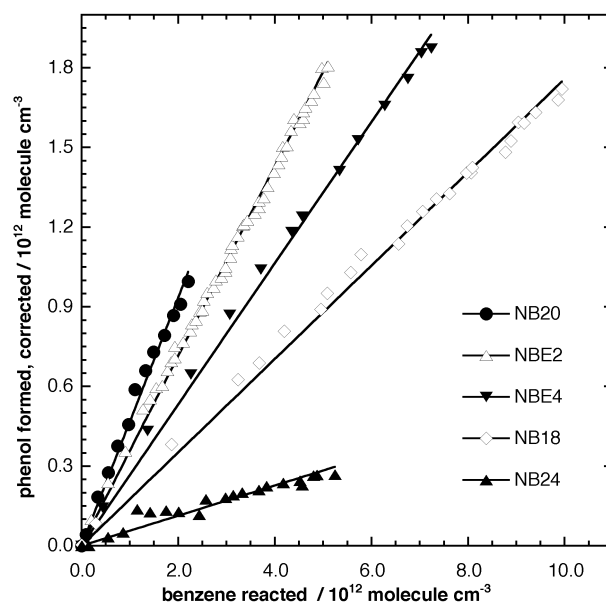


Fig. 2 Proposed mechanisms for the reaction of the hydroxycyclohexadienyl radical **2** with  $\text{NO}_2$  and the hydroxycyclohexadienyl peroxy radical **3** with  $\text{NO}$ . The formation and removal pathways of *E,E*-2,4-hexadienedial **9** are also shown.



**Fig. 3** Product spectra recorded during the photolysis of a benzene/ $\text{NO}_x$  mixture in air (NIES). Product spectra of (a) a low- $\text{NO}_x$  ( $[\text{NO}_x] = 60$  ppb), (b) a high-NO ( $[\text{NO}] = 10\,000$  ppb) and (c) a high- $\text{NO}_2$  ( $[\text{NO}_2] = 7500$  ppb) experiment, after 75 min irradiation and subtraction of the absorptions of the reactants and well characterised products; reference spectra of (d) nitrobenzene, (e) *E,E*-2,4-hexadienedial and (f) phenol. (g)–(i): Spectra (a)–(c) after subtraction of all identified absorptions. Note that for easier comparison, the spectra are normalised by the benzene consumption.

phenol is formed in the presence of high concentrations of NO, which is in line with the expectation from eqn. (1). Instead, a new product dominates the product spectrum; *E,E*-2,4-hexadienedial **9**, compare panel (e). The high- $\text{NO}_2$  experiment shown in panel (c) shows significant absorptions of both phenol and *E,E*-2,4-hexadienedial, qualitatively confirming the indirect results of Atkinson *et al.*<sup>16</sup> that reaction (10) does contribute to phenol formation. Panels (g)–(i) show spectra (a)–(c) after subtraction of the absorption of all identified products. From the spectra shown in Fig. 3 it is evident that under the different experimental conditions employed different products are formed. The dependence of the phenol formation yield on the NO concentration is illustrated in Fig. 4, which shows plots of the phenol formed as a function of the benzene reacted. All phenol concentrations were corrected for losses through OH radical reaction and wall deposition, the amount of benzene reacted has been calculated from the degradation of di-*n*-butyl ether, which served as the OH tracer substance. Of the experiments plotted in Fig. 4, NB24 has the highest average NO concentration. The average NO concentration in the experiments decreased in the order  $c_{\text{NO}}(\text{NB24}) > c_{\text{NO}}(\text{NB18}) > c_{\text{NO}}(\text{NBE4}) > c_{\text{NO}}(\text{NBE2}) > c_{\text{NO}}(\text{NB20})$ , see Table 1. From Fig. 4 it is evident that as the NO concentration increases, the phenol yield decreases.



**Fig. 4** Plots of the phenol formed as a function of benzene reacted for experiments with different average NO concentrations (solid circles: NIES, open circles: FORD, open diamond: EUPHORE). Among these experiments NB20 has the lowest average NO concentration followed by NBE2, NBE4, NB18 and NB24, see Table 1.

### 3.1 Determination of $k_{12}$

As outlined in section 2.6, the phenol yields measured in the high-NO experiments can be used to measure the rate coefficient of the reaction of **3** with NO ( $k_{12}$ ). Fig. 5 shows a plot according to eqn. (6), the slope of which gives  $k_{12}$ . Only the experiments with average NO concentrations above  $10^{13}$  molecule  $\text{cm}^{-3}$  have been considered. Experiments in which either the correction for the  $\text{NO}_2$  reaction of **2** or the uncertainty in the phenol yield exceed 35% are not plotted. The solid line in Fig. 5 represents a non-weighted linear least squares fit through the data plotted, with the intercept fixed at  $k_{\text{clean}} = 760 \text{ s}^{-1}$ . The slope gives:

$$k_{12} = (1.7 \pm 0.6) \times 10^{-11} \text{ cm}^3 \text{ molecule}^{-1} \text{ s}^{-1}.$$

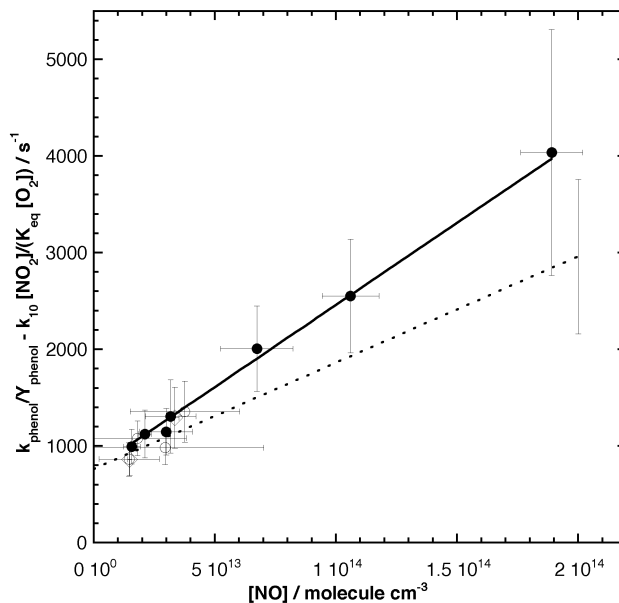


**Fig. 5** Plot according to eqn. (6). The slope gives the rate coefficient of the reaction of the hydroxycyclohexadienyl peroxy radical **3** with NO, see text. The dotted line shows previous results of Bohn and Zetzsch.<sup>8</sup>

Including the low- $\text{NO}_x$  experiments would have the same effect as fixing the intercept at  $k_{\text{clean}}$ , since the value for  $k_{\text{phenol}} = (404 \pm 50) \text{ s}^{-1}$  employed is itself based on  $k_{\text{clean}} = 760 \text{ s}^{-1}$ . The dotted line represents the previous determination of  $k_{12} = (1.1 \pm 0.4) \times 10^{-11} \text{ cm}^3 \text{ molecule}^{-1} \text{ s}^{-1}$  by Bohn and Zetzsch.<sup>8</sup> The value of  $k_{12}$  determined herein is, within the admittedly large uncertainties, indistinguishable from that reported by Bohn and Zetzsch.<sup>8</sup> In Fig. 5 the error limit of  $k_{12}$  reported by Bohn and Zetzsch is shown for one data point. The uncertainty in the present study is the result of the combined uncertainties of the parameters  $k_{\text{phenol}}$ ,  $Y_{\text{phenol}}$ ,  $k_{10}$ ,  $[\text{NO}_2]$ ,  $K_{\text{eq}}$  and  $k_{\text{clean}}$ , which all affect the determination of  $k_{12}$ , see eqn. (6). None of these individual sources of uncertainty dominate the final uncertainty associated with  $k_{12}$ , and consequently a more precise determination of  $k_{12}$  by the method used here will require more precise measurements of all or most of the above parameters. In the discussions below, we choose to adopt the value of  $k_{12}$  measured herein as the value is more compatible with our experimental results (see section 3.2). Finally, it is worth noting that  $k_{12}$  is of a similar magnitude to that of the reaction of other peroxy radicals which typically lie in the range  $(1\text{--}2) \times 10^{-11} \text{ cm}^3 \text{ molecule}^{-1} \text{ s}^{-1}$ .<sup>27</sup>

### 3.2 Phenol yield, $\text{NO}_x$ dependence

As outlined in section 2.5, the phenol yield in the OH initiated oxidation of benzene should be a linear function of the inverse total degradation rate of the hydroxycyclohexadienyl and hydroxycyclohexadienyl peroxy radicals **2** and **3**,  $k_{\text{total}}$ , see eqn. (3). Fig. 6 shows a plot according to eqn. (3), with the phenol yields being corrected for phenol formed through channel (10) in Fig. 1, as determined below. Low values for  $k_{\text{total}}^{-1}$  represent high concentrations of  $\text{NO}_x$ , while the maximum value of  $k_{\text{total}}^{-1} = 1.32 \times 10^{-3} \text{ s}$  represents  $\text{NO}_x$ -free conditions. The phenol yield of Bjergbakke *et al.*<sup>10</sup> and the yield

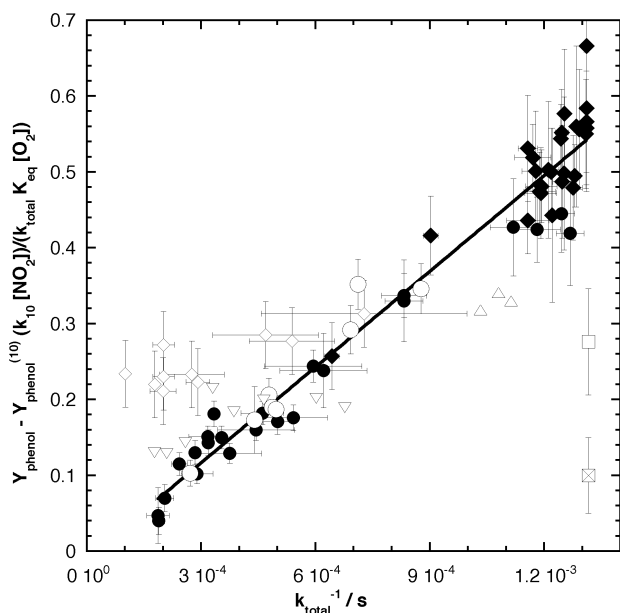


**Fig. 6** Plot of the phenol yield, corrected for phenol formed through reaction (10) (see Fig. 1), as a function of the inverse total degradation rate of **2/3**, see eqn. (3). Data were taken from: NIES experiments, solid circles; EUPHORE experiments, solid diamonds; FORD experiments, hollow circles; Atkinson *et al.*,<sup>16</sup> hollow diamonds; re-evaluated value<sup>7</sup> of Berndt *et al.*,<sup>13</sup> hollow square; re-evaluated value<sup>7</sup> of Bjergbakke *et al.*,<sup>10</sup> crossed square; Berndt and Böge<sup>17</sup> (100 mbar, 295 K), hollow triangle with tip facing down; Berndt and Böge<sup>17</sup> (500 mbar, 293 K), hollow triangle with tip facing up. The line represents a non-weighted linear least squares fit to the data obtained in the present study (NIES, EUPHORE, FORD).

reported by Berndt *et al.*<sup>13</sup> were re-evaluated to match the calibration of this work, see Volkamer *et al.*<sup>7</sup> The  $\text{NO}_x$  concentrations for Atkinson *et al.*<sup>16</sup> were calculated as the averages of the data points reported for each experiment, the yields were calculated by dividing the reported amount of phenol formed, corrected for losses through OH radical reaction, by the reported amount of benzene reacted. The phenol yields of Atkinson *et al.*<sup>16</sup> are also corrected for phenol formation through reaction (10), using the phenol yield from this reaction determined in the present study. The data of Berndt and Böge<sup>17</sup> were also corrected to match the IR absorption cross sections<sup>18</sup> used in the present work.

For the data of the present study as well as those of Atkinson *et al.*<sup>16</sup> the error limits for  $k_{\text{total}}^{-1}$  are calculated using the standard deviation of the measured  $\text{NO}_x$  concentrations as the only source of uncertainties. In addition to these non-systematic errors the inaccuracies of the parameters  $k_{10}$ ,  $k_{12}$ ,  $k_{\text{clean}}$  and  $K_{\text{eq}}$  add to the overall errors. The errors of the phenol yields of Atkinson *et al.*<sup>16</sup> were assumed to be the same as those reported for the average phenol yield, *i.e.* 4.4%. The errors of the phenol yields of the present study were calculated as described earlier.<sup>7</sup>

The observed strong dependence of the phenol yield on the concentration of  $\text{NO}_x$ , while supporting the work of Knispel *et al.*<sup>9</sup> and Bohn and Zetzsch,<sup>8</sup> is in contradiction to the findings of Atkinson *et al.*,<sup>16</sup> the only previous study that employed high concentrations of  $\text{NO}_x$  under comparable experimental conditions. As evident from Fig. 6, the phenol yields reported by Atkinson *et al.* do not show a dependence on the concentration of  $\text{NO}_x$ . This absence of a  $\text{NO}_x$  dependence was supported by two recent studies<sup>13,10</sup> under  $\text{NO}_x$ -free conditions, in which measured phenol yields were in apparent agreement with those reported by Atkinson *et al.*<sup>16</sup> However, as demonstrated in Table 3 of Volkamer *et al.*<sup>7</sup> considerable scatter becomes apparent among these values if the latter two studies are placed on the same basis of calibration.

The absence of  $\text{NO}_x$  dependence of the phenol yield in the data of Atkinson was explained by speculating that a significant yield of phenol in the reaction of the hydroxycyclohexadienyl radical **2** with  $\text{NO}_2$  (reaction (10)) can offset the effect of  $\text{NO}_x$  reactions to lower the phenol yield. A possible mechanism for this is shown in Fig. 2. There is no reasonable mechanism to explain phenol formation from reaction (12), hydroxycyclohexadienyl peroxy +  $\text{NO}$ , see Fig. 2. Though the results of Atkinson *et al.*<sup>16</sup> also qualitatively confirm eqn. (1) under conditions of high  $\text{NO}_x$  considerable differences are found with respect to the phenol yield from channel (10) (see section 3.4).

It may be speculated that these different results are caused by the fact that Atkinson *et al.*<sup>16</sup> used an off-line analytical technique. Atkinson *et al.*<sup>16</sup> used Tenax tubes to adsorb phenol and other compounds, followed by thermal desorption into a GC/FID instrument. The thermal desorption process may have facilitated chemical reactions on the Tenax. For example, intermediates like the nitro hydroxycyclohexadiene **7** or the hydroxycyclohexadiene nitrate **12** (Fig. 2) are probably thermally unstable and may readily eliminate nitrous and nitric acid, respectively, to form phenol. The nitrate **12** may be formed by reaction of the oxyl radical **7** with  $\text{NO}_2$  in both the high- $\text{NO}$  and the high- $\text{NO}_2$  systems, while **7** can be formed by addition of  $\text{NO}_2$  to the hydroxycyclohexadienyl radical **2**, see Fig. 2. These compounds may also photolyse or decompose thermally in the gas-phase.

The hypothesis of thermal/photolytic decomposition of the intermediate **7** may also explain the fact that Atkinson observed the formation of nitrobenzene, which was not observed in the present study, even though it is known to be relatively unreactive.<sup>5</sup> Nitrobenzene can be formed by elimination of  $\text{H}_2\text{O}$  from **7**. Atkinson *et al.*<sup>16</sup> reported yields of nitrobenzene of up to 10% under conditions of very high  $\text{NO}_x$ .

concentrations (10 ppm NO<sub>2</sub>), and extrapolated a nitrobenzene yield of (3.4 ± 0.8)% for NO<sub>x</sub>-free conditions. Atkinson *et al.* noted that this result was not compatible with accepted mechanisms for benzene photooxidation and suggested several alternative schemes, one of them being further reaction of a precursor species. If this precursor species reacts predominantly on the sampling material, this hypothesis can explain why the present study, which employs *in situ* analytical techniques, did not observe nitrobenzene. However, it cannot explain why Berndt and Böge<sup>17</sup> also observed formation of nitrobenzene, even though they used *in situ* FTIR detection, and NO<sub>x</sub>/O<sub>2</sub> ratios that were in the same range as in the present study. The fact that at the spectral resolution of 8 cm<sup>-1</sup> employed in Berndt and Böge<sup>17</sup> many of the nitrate absorptions observed in the present study may become indistinguishable from nitrobenzene absorptions may play a role here. In contrast to the result of Berndt *et al.*<sup>13</sup> the phenol yields of Berndt and Böge<sup>17</sup> are in broad agreement with the present study. This is somewhat surprising because they were measured with the same experimental set-up. However, it should be noted that at high NO<sub>x</sub>/O<sub>2</sub> ratios the 100 mbar data show phenol yields up to 2 times higher than observed in the present study, while the phenol yield at the lowest NO<sub>x</sub>/O<sub>2</sub> ratio is below our values. This becomes clearer in Fig. 4 of Berndt and Böge,<sup>17</sup> where a phenol yield of around 20% is extrapolated for low concentrations of NO<sub>x</sub>. This is consistent with the previous NO<sub>x</sub>-free study from the same laboratory,<sup>13</sup> but inconsistent with our results. However, the better agreement observed among their experiments conducted in the presence of NO<sub>x</sub> and this work is in line with speculations by Volkamer *et al.*<sup>7</sup> about high radical concentrations to explain remaining differences in the absence of NO<sub>x</sub> and 100 mbar total pressure. In the presence of NO<sub>x</sub> the concentration of peroxy radicals would be expected to be considerably lower. It is also noteworthy that the 500 mbar results of Berndt and Böge, which were measured at lower NO<sub>x</sub>/O<sub>2</sub> ratios, show a significantly higher phenol yield than the NO<sub>x</sub>-free data<sup>13</sup> and the 100 mbar data<sup>17</sup> from the same laboratory. This may be an indication of pressure dependences of reactions in the system which deserve future study.

The solid line in Fig. 6 represents the results of a linear non-weighted least squares fit through the data of this study (NIES, EUPHORE, FORD), giving:

$$Y_{\text{phenol}}^{\text{corr}} = (421 \pm 24) \text{ s}^{-1} k_{\text{total}}^{-1} - (0.010 \pm 0.023)$$

The errors given above are 2 standard deviations of the regression analysis and represent statistical precision only. Including the statistical error above and the average uncertainties in the phenol yields determined in this study, we arrive at  $k_{\text{phenol}} = (421 \pm 39) \text{ s}^{-1}$ . The intercept is not statistically significant, in line with the expectation from eqn. (3). The phenol yield under clean (NO<sub>x</sub>-free) conditions is given by  $k_{\text{phenol}}/k_{\text{clean}}$ . Combining the value of  $k_{\text{phenol}} = (421 \pm 39) \text{ s}^{-1}$  derived above with  $k_{\text{clean}} = (760 \pm 80) \text{ s}^{-1}$ <sup>18</sup> gives  $Y_{\text{phenol}}(\text{NO}_x\text{-free}) = (55.4 \pm 7.8)\%$ . This value is consistent with the phenol yield of (53.1 ± 6.6)% calculated from the low-NO<sub>x</sub> experiments reported in part I of this series.<sup>7</sup> Possible explanations for why the NO<sub>x</sub>-free data of Bjergbakke *et al.*<sup>10</sup> and Berndt *et al.*<sup>13</sup> deviate significantly from our results have been given by Volkamer *et al.*,<sup>7</sup> and are not repeated here.

### 3.3 Phenol yield, O<sub>2</sub> dependence

The yield of phenol in the OH initiated oxidation of benzene was found to be independent of the concentration of O<sub>2</sub> in a single experiment (BE31) conducted at EUPHORE at low concentrations of NO<sub>x</sub>.<sup>7</sup> This behaviour is in agreement with eqn. (1) under conditions where reactions (10) and (12) are essentially unimportant. However, at high concentrations of NO<sub>2</sub>

a higher O<sub>2</sub> concentration is expected to result in a higher yield of phenol, even when the NO<sub>x</sub> concentration remains constant. To test this prediction of eqn. (1) a series of experiments was conducted using the smaller chamber at FORD, where the O<sub>2</sub> concentration could be easily varied. In the EUPHORE BE31 experiment the oxygen concentration was raised to 40%, twice the value in normal air. At FORD, oxygen concentrations of 7%, 20% and 93% were employed at a total pressure of 700 Torr, see Experimental section.

As evident from the data given in Table 1, changes in the oxygen concentration were found to have a strong effect on the phenol yield in the high-NO<sub>x</sub> experiments conducted at FORD, but not in the low-NO<sub>x</sub> EUPHORE experiment BE31. In the presence of high concentrations of NO<sub>x</sub>, decreased oxygen concentration leads to decreased phenol yield while increased oxygen concentration leads to increased phenol yield, in line with the prediction from eqn. (1). Also, the effect is observed to be stronger at higher concentrations of NO<sub>x</sub>. In Fig. 6 the low and high O<sub>2</sub> FORD-data are plotted together with the other data obtained in this study and no deviation from the expected quantitative behaviour is observed. The results of these experiments serve as an additional quantitative confirmation of the validity of eqn. (1).

The O<sub>2</sub> dependence of the phenol yield at high concentrations of NO<sub>x</sub> indicates that pathway (5) in Fig. 1, formation of phenol by elimination of an H-atom from the hydroxycyclohexadienyl radical **2**, does not play a significant role in the OH initiated oxidation of benzene. This finding is in line with the results of Bohn and Zetzsch,<sup>8</sup> but contradicts the report by Bjergbakke *et al.*<sup>10</sup>

### 3.4 Phenol yield from reaction (10)

When comparing the product spectra of the high-NO and high-NO<sub>2</sub> experiments (Panels b and c in Fig. 3) it becomes clear that in the high-NO<sub>2</sub> experiments substantial amounts of phenol are formed even though channels (3)–(6) in Fig. 1 are only of secondary importance, see Table 2. This shows that phenol is a product of the reaction of the hydroxycyclohexadienyl radical **2** with NO<sub>2</sub>. A quantitative calculation using the methodology described in section 2.7 gives an average phenol yield for this reaction of  $Y_{\text{phenol}}^{(10)} = (5.9 \pm 3.4)\%$ . The phenol yields calculated for each individual experiment are given in Table 2.

The reaction of the hydroxycyclohexadienyl radical **2** with NO<sub>2</sub> contributes to phenol formation, but not as much as required for the high-NO<sub>x</sub> data of Atkinson *et al.*<sup>16</sup> to be compatible with our results. Using the data of Atkinson *et al.*<sup>16</sup> the phenol yield from channel (10) is calculated to be  $Y_{\text{phenol}}^{(10)} = (18 \pm 6)\%$ ,<sup>28</sup> this is not compatible with the results from this work. As discussed in section 3.2, we believe that there were confounding sources of phenol in the experiments of Atkinson *et al.*<sup>16</sup> Our hypothesis about thermal decomposition of nitrohydroxycyclohexadiene **7** and/or hydroxycyclohexadiene nitrate **12** contributing to the phenol formation in their work is supported by an experiment conducted under conditions of extremely high concentrations of NO<sub>2</sub> and NO (25 ppm each), performed at FORD. Under these conditions the phenol yield became significantly higher at longer reaction times (higher benzene decompositions) rising from 4.3% initially to about 20%. This value is essentially the value<sup>28</sup> estimated from the data of Atkinson *et al.*<sup>16</sup> but cannot be explained by the chemical mechanisms shown in Fig. 1 and 2. The NO<sub>2</sub> concentration fell somewhat during the experiment, while the concentration of NO<sub>x</sub> rose due to the supply of NO by photolysis of CH<sub>3</sub>ONO. Consequently phenol yields would be expected to become lower with the falling concentration of NO<sub>2</sub> and rising concentration of NO, unless an additional mechanism for phenol formation is operative under these extreme conditions.

**Table 2** Summary of the results of the experiments conducted with large excesses of either NO or NO<sub>2</sub>. Columns 3 and 4, respectively, give the phenol and *E,E*-2,4-hexadienedial yields from reaction (10) in Fig. 1. Column 5 gives the yield of *E,E*-2,4-hexadienedial from reaction (12)

Experiment code	Experiment type	$Y_{\text{phenol}}^{(10)}$ (%)	$Y_{E,E-2,4\text{-hexadienedial}}^{(10)}$ (%)	$Y_{E,E-2,4\text{-hexadienedial}}^{(12)}$ (%)	Branching ratio (%) for reaction of 2/3 with		
					O <sub>2</sub>	NO	NO <sub>2</sub>
NB17	High-NO	—	—	27.3 ± 14.0	34	30	37
NB18	High-NO	—	—	31.2 ± 15.9	24	49	27
NB22	High-NO	—	—	29.3 ± 15.4	29	43	29
NB23	High-NO	—	—	30.5 ± 15.6	22	52	26
NB24	High-NO	—	—	26.4 ± 13.2	14	67	19
NB25	High-NO	—	—	31.3 ± 15.7	16	66	19
NB30	High-NO <sub>2</sub>	4.2 ± 2.7	—	—	24	18	58
NB31	High-NO <sub>2</sub>	4.1 ± 2.5	—	—	38	5	57
NB32	High-NO <sub>2</sub>	6.5 ± 3.5	—	—	25	17	58
NB33	High-NO <sub>2</sub>	6.2 ± 3.8	—	—	41	9	51
NB34	High-NO <sub>2</sub>	6.6 ± 3.8	—	—	35	9	56
NB40	High-NO <sub>2</sub>	6.1 ± 3.3	2.9 ± 1.7	—	27	13	60
NB41	High-NO <sub>2</sub>	6.8 ± 3.7	4.0 ± 2.3	—	22	19	60
NB42	High-NO <sub>2</sub>	6.5 ± 3.5	3.3 ± 1.8	—	18	23	59
Averages		5.9 ± 3.4	3.4 ± 1.9	29 ± 16	—	—	—

### 3.5 Yields of *E,E*-2,4-hexadienedial from reactions (10) and (12)

As evident from Fig. 3(b), the main product of the OH initiated oxidation of benzene identified under conditions of extremely high NO concentrations is *E,E*-2,4-hexadienedial **9**, which is presumably formed through reaction of the hydroxycyclohexadienyl peroxy radical **3** with NO (reaction (12)), see Fig. 2. The yield of *E,E*-2,4-hexadienedial following this reaction was calculated using the methodology described in section 2.8, individual results are shown in Table 2, together with the branching ratios between the loss processes for **2/3** with O<sub>2</sub>, NO and NO<sub>2</sub>. An average value of  $Y_{E,E-2,4\text{-hexadienedial}}^{(12)} = (29 \pm 16)\%$  was determined for the yield of *E,E*-2,4-hexadienedial following reaction (12). Two examples of experimental and fitted concentration–time profiles of *E,E*-2,4-hexadienedial are given in Fig. 7, showing the first and last experiments of the

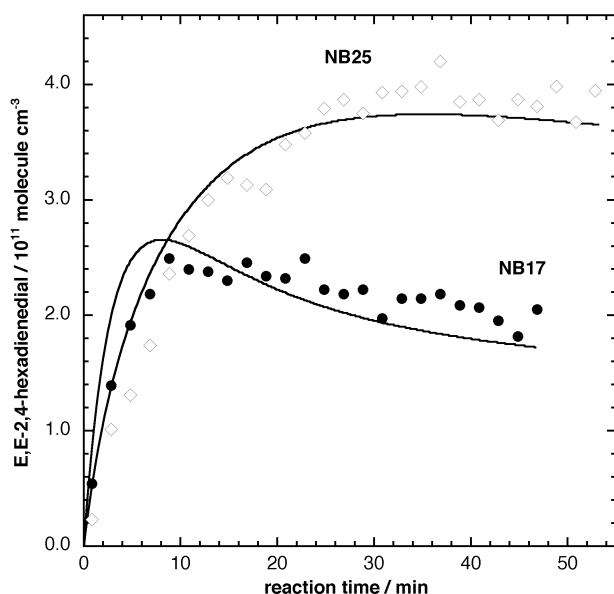


**Fig. 7** Experimental (symbols) and fitted (lines) concentration–time profiles for *E,E*-2,4-hexadienedial in benzene/CH<sub>3</sub>ONO/NO<sub>x</sub> experiments in the presence of high NO concentrations (NIES). The first (NB17, lowest NO) and last (NB25, highest NO) of the series of high-NO experiments are shown.

high-NO series. Experiment NB17 is the one with the lowest initial NO concentration in that series, and consequently the reaction of NO with **3** only accounts for *ca.* 30% of the decay of **2/3**. This represents the experiment with the lowest NO concentration that could be reliably evaluated for *E,E*-2,4-hexadienedial. Experiment NB25, together with NB24, represents the highest NO concentrations employed in this study, about 66% of **2/3** is lost through reaction of **3** with NO. Fig. 7 shows that the chemical mechanism shown in Fig. 2 gives reasonably good fits to the experimental data. The observed deviations, notably the faster rise of the *E,E*-2,4-hexadienedial concentration in the fits, are probably due to the fact that the kinetic parameters employed were obtained under different light conditions that were scaled to the  $J(\text{NO}_2)$  value in the NIES reaction chamber. These uncertainties are estimated at 50% and dominate the errors reported in Table 2.

The formation of *E,E*-2,4-hexadienedial in the high-NO<sub>2</sub> experiments was larger than expected from the reaction of **3** with NO alone, indicating that the reaction of **2** with NO<sub>2</sub> also gives *E,E*-2,4-hexadienedial. A proposed pathway to *E,E*-2,4-hexadienedial formation from this reaction is shown in Fig. 2. Table 2 includes calculated yields for *E,E*-2,4-hexadienedial from the reaction of the hydroxycyclohexadienyl radical **2** with NO<sub>2</sub>, see experimental section. An average value of  $Y_{E,E-2,4\text{-hexadienedial}}^{(10)} = (3.4 \pm 1.9)\%$  is calculated. *E,E*-2,4-hexadienedial is therefore a minor product formed from the reaction of **2** with NO<sub>2</sub> (reaction (10) in Fig. 1).

A simple mechanism for the formation of *E,E*-2,4-hexadienedial **9** in reaction (10) is shown in the left column of Fig. 2. The reaction of **2** with NO<sub>2</sub> can proceed *via* oxygen transfer to the carbon ring, giving a hydroxycyclohexadienyl oxyl radical **8** and NO, as proposed by Zellner *et al.*<sup>25</sup> The hydroxycyclohexadienyl oxyl radical **8** can then give *Z,Z*-2,4-hexadienedial **9a** by ring cleavage and abstraction of an H-atom by molecular oxygen. *Z,Z*-2,4-hexadienedial **9a** will rapidly isomerise into its more stable *E,E*-form **9**.<sup>23,24</sup> Alternatively, the delocalised pentadienyl-type radical formed after ring-opening of **8** can isomerise before reaction with O<sub>2</sub>, resulting in the direct formation of *E,E*-2,4-hexadienedial **9**. The most likely formation mechanism for *E,E*-2,4-hexadienedial from reaction (12), based on the work of Hoshino *et al.*,<sup>26</sup> is given in the right column of Fig. 2. Reaction of NO with **3** gives a hydroxycyclohexadienyl oxyl radical **8**, which can then give *E,E*-2,4-hexadienedial as described above.

The yields determined for the individual experiments shown in Table 2 do not show any systematic variation with the

concentration of  $\text{NO}_x$ , even though in the high- $\text{NO}$  experiments the relative importance of the reaction of **2/3** with  $\text{O}_2$  and  $\text{NO}$  changes by about a factor of 2. This indicates that within the experimental errors *E,E*-2,4-hexadienedial is not formed in the absence of  $\text{NO}_x$ . While this is expected from the reaction mechanism shown in Fig. 1, it appears to be in contradiction to the results of Berndt *et al.*<sup>13</sup> and Berndt and Böge.<sup>17</sup> The FTIR spectra shown by Berndt *et al.*,<sup>13</sup> measured under  $\text{NO}_x$ -free conditions, seem to show significant absorptions of *E,E*-2,4-hexadienedial. In part I of this series<sup>7</sup> it was speculated that the very high radical concentrations in that system may have led to a different chemistry of the intermediates **2/3**, leading to the formation of *E,E*-2,4-hexadienedial through pathways not occurring under atmospheric conditions. In the more recent  $\text{NO}_x$  dependent study of Berndt and Böge,<sup>17</sup> a maximum *E,E*-2,4-hexadienedial yield of about 36% of the benzene reacted was found at very high concentrations of  $\text{NO}_x$ , using an estimated absorption cross section. When this yield is re-calibrated using the FTIR absorption cross section of Etzkorn *et al.*<sup>18</sup> a value of 17% is obtained. When it is further considered that a maximum of about 70% of **2/3** reacts with  $\text{NO}$  under the experimental conditions of Berndt and Böge,<sup>17</sup> a yield of 24% is obtained for the formation of *E,E*-2,4-hexadienedial from reaction (12). This compares well with the value of  $(29 \pm 16)\%$  found here. The *E,E*-2,4-hexadienedial yields of Berndt and Böge drop significantly at low  $\text{NO}_x$  concentrations (see their Fig. 4), though there appears to be a statistically significant *E,E*-2,4-hexadienedial formation of about 10% (re-calibrated 7%) under  $\text{NO}_x$ -free conditions. This is consistent with Berndt *et al.*,<sup>13</sup> but not with the results of the present study.

The error limits of the *E,E*-2,4-hexadienedial yields reported in Table 2 are a combination of an estimated uncertainty of 50% resulting from the degradation kinetics of this compound, and the 2-sigma errors from the fitting procedure described in section 2.8. The atmospheric chemistry of *E,E*-2,4-hexadienedial was not determined in our laboratory but was adapted from the literature,<sup>23,24</sup> the error is therefore largely systematic in nature. However, the good agreement with the value determined by Berndt and Böge,<sup>17</sup> whose experimental set-up is far less susceptible to secondary chemistry than that reported herein, indicates that our estimated uncertainty of 50% is very conservative. The statement on the absence of *E,E*-2,4-hexadienedial formation under  $\text{NO}_x$ -free conditions is more precise. Our data regarding the absence of hexadienedials at low concentrations of  $\text{NO}_x$  is in agreement with two recent studies<sup>7,14</sup> which observed no indication for the formation of hexadienedials in the presence of low concentrations of  $\text{NO}_x$  (several tens ppb). Under these conditions an upper limit for the yield of hexadienedials from benzene of 8% was derived.<sup>14</sup>

### 3.6 Other products of reactions (10) and (12)

The only product identified in the reaction of the hydroxycyclohexadienyl peroxy radical **3** with  $\text{NO}$  (reaction (12)) was *E,E*-2,4-hexadienedial **9** with a yield of  $(29 \pm 16)\%$ , no other products were observed which could be unequivocally attributed to this reaction. In the case of the reaction of the hydroxycyclohexadienyl radical **2** with  $\text{NO}_2$  (reaction (10)), only two products were observed; phenol **4** and *E,E*-2,4-hexadienedial **9** in yields of a few percent each. Thus the major fraction of the products of both reactions could not be identified, and only minor products of reaction (10) were found.

Panels (g), (h), and (i) of Fig. 3 show residual product spectra obtained in the 3 types of experiments performed at NIES. These residual spectra were obtained by subtracting the absorptions of all reactants and identified products from the product spectra shown in panels (a), (b) and (c). The product spectra were normalised by the benzene consumption to allow an easier comparison, which again results in different levels of

spectral noise. It is noteworthy that the residual spectra in the two types of high- $\text{NO}_x$  experiments are similar, both in terms of the absorptions and their relative intensities, while the residual spectrum of the low- $\text{NO}_x$  experiment in panel (g) is significantly less intense and shows different absorptions. This reflects the fact that 97% of the loss of **2** and **3** in this experiment is through reaction with  $\text{O}_2$ , and only 3% through reactions with  $\text{NO}$  and  $\text{NO}_2$ . The similarity between the residual spectra of the 2 types of high- $\text{NO}_x$  experiments shows that peroxy nitrates, which cannot be formed at high concentrations of  $\text{NO}$ , are not formed in significant yields. Some of the other bands observed in panels (h) and (i) of Fig. 3 are indicative of nitrates, which typically exhibit absorptions in the regions around  $1650\text{ cm}^{-1}$ ,  $1300\text{ cm}^{-1}$ ,  $850\text{ cm}^{-1}$  and  $1000\text{ cm}^{-1}$  (some only). The residual spectra of the high- $\text{NO}_x$  experiments show bands around those regions, the nitrate band expected around  $1650\text{ cm}^{-1}$  may be obscured by saturated absorptions of  $\text{NO}_2$ . The formation of nitrates in the reaction of peroxy radicals with  $\text{NO}$  has been known for some time.<sup>29</sup> It is also established that the nitrate yield increases with size of the peroxy radical. Nitrate yields of approximately 20% are observed in the reaction of hexylperoxy radicals with  $\text{NO}$ .<sup>27,30</sup> It is reasonable to expect a substantial nitrate yield in reaction (12).

Other absorptions are visible in the carbonyl region. The band visible at  $1830\text{ cm}^{-1}$  is typical of electron rich carbonyl groups, *e.g.* in  $\text{R-CO-O-R}$ . Additional strong bands at  $1680$ ,  $1707$  and  $1750\text{ cm}^{-1}$  indicate the presence of further carbonyls and unsaturated carbonyls. In contrast to the region below  $1600\text{ cm}^{-1}$  the carbonyl regions exhibit similar absorptions in the 3 systems studied. There are a few similarities between the residual product spectra recorded here under high- $\text{NO}_x$  conditions and the residual product spectra of the OH initiated oxidation of hexadienedial isomers reported in the literature.<sup>23</sup> It seems likely that some of the residual absorptions shown in panels (h) and (i) of Fig. 3 are attributable to products of the further reaction of *E,E*-2,4-hexadienedial.

One product that has been reported previously as arising from the OH initiated oxidation of benzene in the presence of  $\text{NO}_x$  is nitrobenzene **13**, which can be formed as shown in Fig. 2. By comparison of panel (d) with panels (a)–(c) in Fig. 3 it is evident that nitrobenzene, which is essentially unreactive, is not formed above its detection limit. It is concluded that, even at extremely high  $\text{NO}_x$  concentrations, nitrobenzene is formed in a yield below the value of  $(3.4 \pm 0.8)\%$  extrapolated for  $\text{NO}_x$ -free conditions by Atkinson *et al.*,<sup>16</sup> who determined yields of up to 10% under conditions of high concentrations of  $\text{NO}_x$ . Possible reasons for this and other discrepancies are discussed in section 3.2. The absence of nitrobenzene in the present study is in contradiction to the recent results of Berndt and Böge,<sup>17</sup> who found a yield of 11% at high concentrations of  $\text{NO}_x$ . This may again be an indication that additional mechanisms are operative under the conditions of that study. The results of Berndt and Böge are generally compatible with those of Atkinson, with the exception of nitrobenzene formation at low concentrations of  $\text{NO}_x$ , which Berndt and Böge do not observe.

In summary, less than one third of the products of the reaction of the hydroxycyclohexadienyl peroxy radical **3** with  $\text{NO}$  and less than 10% of the products of the reaction of the hydroxycyclohexadienyl radical **2** with  $\text{NO}_2$  could be identified in the present study. Fig. 2 contains other possible pathways for these reactions, however, phenol and *E,E*-2,4-hexadienedial were the only products that could be identified. 1,2-Dihydroxybenzene **11**, which may result from the reaction of **3** with  $\text{NO}$ , is highly reactive<sup>31</sup> and may be formed in considerable yield without being detectable under the present experimental conditions. On the basis of the residual product spectra shown in Fig. 3, we speculate that nitrates and possibly other nitrogen containing compounds are formed in high yields.

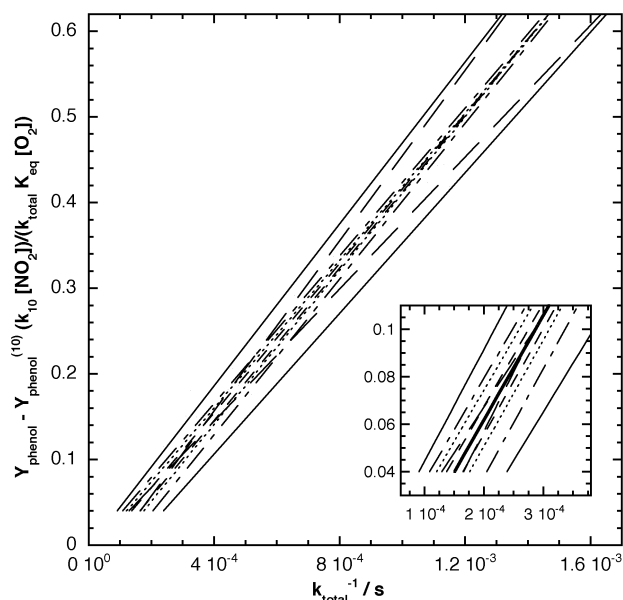


**Fig. 8** Plot according to eqn. (3) showing linear fits through the experimental data when the upper and lower limits of  $k_{10}$ ,  $k_{12}$ ,  $K_{eq}$  and  $k_{clean}$  are used instead of the recommended values. The inset shows an expanded view of the high- $\text{NO}_x$  region (low values of  $k_{total}^{-1}$ ). The calculations of  $k_{total}^{-1}$  were performed with: upper and lower limits of  $k_{12}$ , dash-dot-dash lines; upper and lower limits of  $k_{10}$ , short dashed lines; upper and lower limits of  $k_{clean}$ , long dashed lines; upper and lower limits of  $K_{eq}$ , dotted lines; maximum (lower limits of  $k_{12}$ ,  $k_{10}$  and  $k_{clean}$  and upper limit of  $K_{eq}$ ) and minimum (upper limits of  $k_{12}$ ,  $k_{10}$  and  $k_{clean}$  and lower limit of  $K_{eq}$ ) values of  $k_{total}$ , solid lines; recommended values for  $k_{12}$ ,  $k_{10}$ ,  $k_{clean}$  and  $K_{eq}$ , thick line (inset only).

### 3.7 Error considerations

The influence of the uncertainties in the kinetic parameters  $k_{10}$ ,  $k_{12}$ ,  $k_{clean}$  and  $K_{eq}$  on the data evaluation has been examined. Fig. 8 shows plots of linear fits through the experimental data according to eqn. (3) when the upper and lower limits, respectively, of  $k_{10} = (2.75 \pm 0.2) \times 10^{-11} \text{ cm}^3 \text{ molecule}^{-1} \text{ s}^{-1}$ ,  $k_{12} = (1.7 \pm 0.6) \times 10^{-11} \text{ cm}^3 \text{ molecule}^{-1} \text{ s}^{-1}$ ,  $K_{eq} = (2.7 \pm 0.4) \times 10^{-19} \text{ cm}^3 \text{ molecule}^{-1}$  and  $k_{clean} = (760 \pm 80) \text{ s}^{-1}$  are used instead of the recommended values. The values and their errors are taken from Knispel *et al.*,<sup>9</sup> Bohn and Zetzsch<sup>8</sup> and this work. The inset shows an expanded view of the high- $\text{NO}_x$  region at low values of  $k_{total}^{-1}$ . The individual measured data points are not shown. As expected,  $k_{clean}$  is the dominant source of error in the low- $\text{NO}_x$  region, while the errors associated with  $k_{10}$ ,  $k_{12}$  and  $K_{eq}$  are more important in the high- $\text{NO}_x$  region.

At high- $\text{NO}_x$  the uncertainties in  $K_{eq}$  and especially  $k_{12}$  widely determine the overall uncertainty. Despite the fact that the value of  $k_{10}$  is about twice as high as the value of  $k_{12}$  the uncertainty in  $k_{10}$  only adds a minor error. This is mainly due to the about five times lower relative uncertainty in  $k_{10}$ . For  $K_{eq}$ , its larger uncertainty increases its significance over that of  $k_{10}$ . The black line in Fig. 8 represents upper and lower limits for  $k_{total}^{-1}$ , using either the lower limits of  $k_{10}$ ,  $k_{12}$ ,  $k_{clean}$  and the upper limit of  $K_{eq}$  or the upper limits of  $k_{10}$ ,  $k_{12}$ ,  $k_{clean}$  and the lower limit of  $K_{eq}$ , respectively. The thick black line shows a linear fit to the experimental data using the above values for these constants, to avoid cluttering the graph it is shown in the inset only. It is evident from Fig. 8 that the major contribution to the overall error under conditions of high- $\text{NO}_x$  is due to uncertainty in  $k_{12}$ .

## 4. Conclusions and atmospheric implications

A strong dependence of the phenol yield on the concentrations of  $\text{NO}_x$  was observed in the OH initiated oxidation of benzene,

which is in contradiction to previous studies. The simple formula (1) introduced in part I of this series<sup>7</sup> is confirmed under conditions of high concentrations of  $\text{NO}_x$  (up to  $>10$  ppm). A study of the dependence of the phenol yield on the concentration of  $\text{O}_2$  further confirmed the results and supports previous conclusions<sup>8</sup> that channel (5) in Fig. 1 is not a significant loss process for the hydroxycyclohexadienyl radical, **2**. With this work a complete and consistent set of rate constant and yield data is available to calculate the phenol yield in the OH radical initiated oxidation of benzene in the presence of  $\text{NO}_x$ .

The changes in the chemical mechanism of the OH initiated oxidation of benzene at high concentrations of  $\text{NO}_x$  were confirmed by the products observed under these conditions, which are distinctly different from those observed at low  $\text{NO}_x$  concentrations. Increased importance of the reactions of the hydroxycyclohexadienyl radical **2** with  $\text{NO}_2$  and the hydroxycyclohexadienyl peroxy radical **3** with NO are concluded to be responsible for these differences and dedicated product studies of these reactions were carried out for the first time. *E,E*-2,4-Hexadienedial was observed as a significant product of the latter reaction, small amounts of phenol and *E,E*-2,4-hexadienedial are formed in the former. The kinetic parameters for the initial steps of the OH initiated oxidation of benzene (see Fig. 1) determined by Knispel *et al.*<sup>9</sup> and Bohn and Zetzsch<sup>8</sup> are consistent with the product yields determined in this study. The rate constant for reaction of the hydroxycyclohexadienyl peroxy radical **3** with NO measured herein is higher than the value by Bohn and Zetzsch,<sup>8</sup> their value is at the lower limit of our error margins. The uncertainty in the rate-constant of this reaction limits the conclusions that can be drawn from experiments conducted at high concentrations of  $\text{NO}_x$ .

The observed strong  $\text{NO}_x$ -dependence of the degradation chemistry is in contrast to the chemistry of alkanes and most alkenes, where the formation of peroxy radicals is essentially irreversible. This highlights the special role aromatic hydrocarbon mechanisms hold in atmospheric chemistry.

The results also have important consequences for atmospheric modelling studies. Most chemical models used for the prediction of tropospheric photooxidant formation are verified by comparing their predictions to experimental data from smog-chamber studies conducted at high levels of  $\text{NO}_x$ . Currently, levels of  $\text{NO}_x$  in such studies are typically in the range 100–1000 ppb.<sup>32–34</sup> The results of the present study show that benzene exhibits a distinctly different degradation chemistry in the presence of 1–10 ppm  $\text{NO}_x$  than in the presence of more atmospherically relevant concentrations of 1–100 ppb  $\text{NO}_x$ . This finding is qualitatively transferable to other aromatic hydrocarbons.<sup>28,35</sup> The effect of high concentrations of  $\text{NO}_x$  needs to be taken into account in the verification of chemical models for tropospheric chemistry. Thus, the high- $\text{NO}_x$  chemistry needs to be included in models that are to be validated against existing smog-chamber studies. The new data on product yields and kinetics presented here should allow some progress in this field. Also, future experimental studies aimed at establishing/verifying chemical mechanisms for aromatic hydrocarbons should be performed using  $\text{NO}_x$  levels which are representative of those found in the atmosphere.

## Acknowledgements

The authors are grateful for financial support of this work by the “Bundesministerium für Bildung, Wissenschaft, Forschung und Technologie” (BMBF, grant 07TFS30) and the European Commission (project EXACT, EVK2-1999-00332). B. K. gratefully acknowledges successive fellowships of the Japan Science and Technology Agency (STA)/Alexander von Humboldt Foundation and the Environment Ministry of Japan. R. V. acknowledges a Marie Curie fellowship from

the European Commission, DG-XII. O. J. N. acknowledges financial support from the Danish Natural Science Research Council. Further, the support of Jens Ücker and Milagros Ródenas in the EUPHORE experiments is acknowledged. The CEAM Foundation is supported by the Generalitat Valenciana and the Fundació BANCAIXA.

## References

- 1 J. G. Calvert, R. Atkinson, K. H. Becker, R. M. Kamens, J. H. Seinfeld, T. J. Wallington and G. Yarwood, *Mechanisms of Atmospheric Oxidation of Aromatic Hydrocarbons*, Oxford University Press, Oxford, 2002.
- 2 J. R. Odum, T. P. W. Jungkamp, R. J. Griffin, R. C. Flagan and J. H. Seinfeld, *Science*, 1997, **276**, 96.
- 3 L. Wang, J. B. Milford and W. P. L. Carter, *Atmos. Environ.*, 2000, **34**, 4337.
- 4 L. Wang, J. B. Milford and W. P. L. Carter, *Atmos. Environ.*, 2000, **34**, 4349.
- 5 R. Atkinson, *J. Phys. Chem. Ref. Data*, 1994, Monograph No. 2, 1.
- 6 S. D. Piccot, J. J. Watson and J. W. Jones, *J. Geophys. Res.*, 1992, **97**, 9897.
- 7 R. Volkamer, B. Klotz, I. Barnes, T. Imamura, K. Wirtz, N. Washida, K. H. Becker and U. Platt, *Phys. Chem. Chem. Phys.*, 2002, **4**, 1598.
- 8 B. Bohn and C. Zetzsch, *Phys. Chem. Chem. Phys.*, 1999, **1**, 5097.
- 9 R. Knispel, R. Koch, M. Siese and C. Zetzsch, *Ber. Bunsen-Ges. Phys. Chem.*, 1990, **94**, 1375.
- 10 E. Bjergbakke, A. Sillesen and P. Pagsberg, *J. Phys. Chem.*, 1996, **100**, 5729.
- 11 R. Koch, *J. Phys. Chem. B*, 1997, **101**, 293.
- 12 P. Pagsberg, *J. Phys. Chem. B*, 1997, **101**, 294.
- 13 T. Berndt, O. Böge and H. Herrmann, *Chem. Phys. Lett.*, 1999, **314**, 435.
- 14 R. Volkamer, U. Platt and K. Wirtz, *J. Phys. Chem. A*, 2001, **105**, 7865.
- 15 F. Berho and R. Lesclaux, *Phys. Chem. Chem. Phys.*, 2001, **3**, 970.
- 16 R. Atkinson, S. M. Aschmann, J. Arey and W. P. L. Carter, *Int. J. Chem. Kinet.*, 1989, **21**, 801.
- 17 T. Berndt and O. Böge, *Phys. Chem. Chem. Phys.*, 2001, **3**, 4946.
- 18 T. Etkorn, B. Klotz, S. Sørensen, I. V. Patroescu, I. Barnes, K. H. Becker and U. Platt, *Atmos. Environ.*, 1999, **33**, 525.
- 19 B. Klotz, S. Sørensen, I. Barnes, K. H. Becker, T. Etkorn, R. Volkamer, U. Platt, K. Wirtz and M. Martín-Reviejo, *J. Phys. Chem. A*, 1998, **102**, 10289.
- 20 H. Akimoto, M. Hoshino, G. Inoue, F. Sakamaki, N. Washida and M. Okuda, *Environ. Sci. Technol.*, 1979, **13**, 471.
- 21 T. J. Wallington and S. M. Japar, *J. Atmos. Chem.*, 1989, **9**, 399.
- 22 W. P. L. Carter, A. M. Winer and J. N. Pitts, Jr., *Environ. Sci. Technol.*, 1981, **15**, 829.
- 23 B. Klotz, A. Bierbach, I. Barnes and K. H. Becker, *Environ. Sci. Technol.*, 1995, **29**, 2322.
- 24 B. Klotz, I. Barnes and K. H. Becker, *Int. J. Chem. Kinet.*, 1999, **31**, 689.
- 25 R. Zellner, B. Fritz and M. Preidel, *Chem. Phys. Lett.*, 1985, **121**, 412.
- 26 M. Hoshino, H. Akimoto and M. Okuda, *Bull. Chem. Soc. Jpn.*, 1978, **51**, 718.
- 27 P. D. Lightfoot, R. A. Cox, J. N. Crowley, M. Destriau, G. D. Hayman, M. E. Jenkin, G. K. Moortgat and F. Zabel, *Atmos. Environ. A*, 1992, **26**, 1805.
- 28 R. Volkamer, PhD thesis, University of Heidelberg, <http://www.ub.uni-heidelberg.de/archiv/1939>, 2001.
- 29 R. Atkinson, *J. Phys. Chem. Ref. Data*, 1997, **26**, 215.
- 30 J. Arey, S. M. Aschmann, E. S. C. Kwok and R. Atkinson, *J. Phys. Chem. A*, 2001, **105**, 1020.
- 31 R. Olariu, I. Barnes, K. H. Becker and B. Klotz, *Int. J. Chem. Kinet.*, 2000, **32**, 696.
- 32 W. R. Stockwell, F. Kirchner, M. Kuhn and S. Seefeld, *J. Geophys. Res.*, 1997, **102**, 25847.
- 33 M. C. Dodge, *Atmos. Environ.*, 2000, **34**, 2103.
- 34 M. Jang and R. M. Kamens, *Environ. Sci. Technol.*, 2001, **35**, 3626.
- 35 R. Volkamer, J. Uecker, K. Wirtz and U. Platt, *Proc. EURO-TRAC II Symposium*, 11th–15th March 2002, Garmisch-Partenkirchen, Germany.